Molecular Catalysis xxx (xxxx) xxx–xxx

Contents lists available at ScienceDirect

Molecular Catalysis

journal homepage: www.elsevier.com/locate/mcat

Selective lactose oxidation in aqueous-phase over Ag-Au bimetallic nanoparticles supported on Al_2O_3 under mild reaction conditions

C.I. Meyer[a,*], S.A. Regenhardt[a], H.A. Duarte[a], J. Zelin[a], V. Sebastian[b,c], T.F. Garetto[a], A.J. Marchi[a]

[a] Catalysis Science and Engineering Research Group (GICIC), INCAPE, UNL-CONICET, Colectora Ruta Nacional Nº 168, Km 0, 3000, Santa Fe, Argentina
[b] Department of Chemical Engineering, Aragon Institute of Nanoscience (INA), University of Zaragoza, Campus Río Ebro-Edificio I+D, C/ Poeta Mariano Esquillor S/N, 50018, Zaragoza, Spain
[c] CIBER de Bioingeniería, Biomateriales y Nanomedicina (CIBER-BBN), C/Monforte de Lemos 3-5, Pabellón 11, 28029, Madrid, Spain

ARTICLE INFO

Keywords:
Lactose
Ag-Au nanoparticles
Catalytic selective oxidation
Lactobionic acid
Kinetic study

ABSTRACT

In this work, Au-Ag based catalysts supported on Al_2O_3 were prepared by a precipitation-deposition method at controlled pH and tested in the selective lactose (LA) oxidation to lactobionic acid (LB) in aqueous phase. Combining XPS and STEM-HAADF, it was found that there is an important surface Ag enrichment of bimetallic nanoparticles for bulk atomic ratios Au/(Au + Ag) > 0.5. These bimetallic nanoparticles were active for the selective LA oxidation into LB and the maximum activity was reached with Au/(Au + Ag) = 0.9. In this case, the surface Au/(Au + Ag) atomic ratio was about 0.5, which indicates that there is the same amount of both elements at the active surface of the catalyst. Assuming that LA is chemisorbed on Au sites, and O_2 on Ag ones, this particular surface atomic ratio would favor the interaction and reaction between both reactants. Thus, the synergistic effect between Au and Ag could explain the results of this study. A compensation effect between frequency factor and activation energy supports the existence of such synergy. If the atomic ratio is Au/(Au + Ag) ≤ 0.5, a layer of Ag deposits over the Au nanoparticles (core-shell structure) and the conversion of LA into LB drops to zero.

1. Introduction

Carbohydrates have been widely used in the manufacture of bulk and fine chemicals, and they are considered as a renewable raw material for green chemistry products [1–3]. In this sense, selective oxidation or hydrogenation of sugars, such as glucose, fructose, cellobiose and lactose, have been extensively studied and reviewed [4–8]. The biological oxidations of these carbohydrates are processes that normally require long reaction times to reach high levels of conversion and by-products such as H_2O_2 are formed, which is detrimental to yield in the desired product [9–11]. Particularly, lactose (LA) is a major component of whey (about 5 wt% LA), the main by-product in cheese production. Only a small fraction of the whey produced is processed to obtain LA, while most part is treated as waste. This LA could be converted to added-value compounds either by hydrogenation or oxidation reactions [12–17]. For instance, by selective oxidation, LA can be converted to lactobionic acid (LB). This is an alfa-hydroxy acid with antioxidant and emollient properties, which makes it a high added-value product for food and pharmaceutical industries [13]. As a matter of fact, its largest commercial use is as an important component of the solutions used to preserve human organs during transplant procedures. LB is also employed as acidulant, complexing agent, antioxidant for food, and as an ingredient for skin care or as filler in pharmaceuticals products [9].

There has been an increasing interest in LB production by heterogeneous catalytic oxidation of LA [11–17]. Murzina et al. found that the type of metal, reaction medium, pH, temperature, and O_2 concentration have an important influence on LA oxidation in liquid-phase [13]. Tokarev and Murzina studied extensively the oxidation of LA and glucose using electrochemical catalysis based on metal electrodes [8,12,13]. They carried out kinetics and mechanistic studies over Pd/C catalyst and found an important deactivation of Pd for over-oxidation and self-poisoning. Pt and Pd-based catalysts, in some cases promoted with Bi, were used to carry out the oxidation of sugars [5,6,12,14]. These catalysts were deactivated during the reaction, probably due to the over-oxidation of the metal surface [12].

It is already known that bulk Au catalysts and large Au particles are inert to most of the chemical reactions. Instead, highly dispersed metallic Au nanoparticles are highly active for oxidation reactions. LA oxidation has been studied employing well dispersed Au on inert or reducible supports, and with different acidic properties such as SiO_2,

* Corresponding author.
E-mail address: cmeyer@fiq.unl.edu.ar (C.I. Meyer).

https://doi.org/10.1016/j.mcat.2018.11.020
Received 29 June 2018; Received in revised form 22 November 2018; Accepted 27 November 2018

Al_2O_3, and ZrO_2 [13,15,17]. From the analysis of concentration–time curves in those works, it was claimed that the kinetic order respect to LA was zero. In a previous work, we found that Au nanoparticles supported on Al_2O_3 is a highly selective and stable catalyst to oxidized LA to LB in aqueous phase [17]. We also determined that the apparent order of reaction respect to LA was zero for a given initial concentration of reactant, which is in agreement with the literature. However, using pseudo-homogeneous and LHHW models, a negative order in respect to initial LA concentration was determined. This result would indicate that LA is strongly chemisorbed on the surface of metal Au nanoparticles.

Regarding the selective oxidation of carbohydrates in aqueous phase, to our knowledge, there are few studies in the open literature dealing with the use of bimetallic Ag-Au catalysts for LA oxidation [2,18,19]. For instance, Benkó et al. found that Ag-Au/SiO_2 bimetallic nanoparticles prepared by sol-adsorption method with different Ag/Au ratios were active in glucose oxidation to gluconic acid [18]. They proposed a synergistic effect between Ag-Au to explain the performance of these bimetallic catalysts, with the maximum activity for Ag/Au atomic ratio of 20/80. On the other hand, Zhang et al. prepared unsupported bimetallic catalysts with an Ag core and Au shell structure. These stabilized colloidal nanoparticles with different Ag and Au contents were extensively characterized [19].

The aim of this work is to obtain active, selective and stable supported Ag-Au bimetallic catalysts for LA oxidation in aqueous phase, using the precipitation-deposition method at controlled pH. For this purpose, we prepared a series of Ag-Au samples supported on Al_2O_3 with different Au/(Ag + Au) atomic ratios. The catalytic performance of the monometallic and bimetallic catalysts prepared was analyzed and explained. The influence of the reaction temperature on the LA oxidation over Au-Ag catalysts was also studied. An Arrhenius-like model was used and the estimates obtained for the activation energy and the frequency factor corresponding to each catalyst were analyzed and compared.

2. Experimental

2.1. Catalyst preparation

Monometallic, Au or Ag, and bimetallic Ag-Au catalyst precursors using γ-Al_2O_3 as support were prepared by precipitation-deposition method at controlled pH. The γ-Al_2O_3 (CK 300 Cyanamid Ketjen, S_{BET} = 190 $m^2 g^{-1}$, Vp = 0.49 $cm^3 g^{-1}$) was calcined at 600 °C in air for 6 h before deposition of the metal precursors, in order to remove any type of compounds, e.g. hydrocarbons and others, which can be strongly adsorbed and could hinder the deposition and/or adsorption of catalyst precursors on the support surface. The monometallic samples, Au/Al_2O_3 and Ag/Al_2O_3, were prepared according to the procedure described by Centeno et al. [20]. Bimetallic samples, AgAu/Al_2O_3, were prepared following the same procedure, but in two consecutive steps, as described below. The corresponding amount of $AgNO_3$ (Sigma-Aldrich, 99.99%) was dissolved into 100 mL of deionized water, then heated up to 70 °C and pH was adjusted to 7.0 ± 0.1 with a 0.1 N NaOH aqueous solution. Afterwards, Al_2O_3 was added to this solution and the suspension stirred for 1 h. The slurry obtained was filtrated, washed with hot deionized water and dried in oven at 80 °C overnight. From there on, the corresponding amount of $HAuCl_4{\cdot}3H_2O$ (Sigma-Aldrich, 99.99%) was dissolved into 100 mL of deionized water, heated up to 70 °C, and pH was adjusted to 7.0 ± 0.1 with a 0.1 N NaOH aqueous solution. The solid Ag precursor obtained previously, was incorporated to the solution and the suspension stirred for 1 h. The slurry was filtrated and thoroughly washed with hot deionized water until none Cl-ions were detected in the washing water. The hydrated precursor obtained was dried in oven at 80 °C overnight and calcined in air at 500 °C for 2 h in a muffle furnace. Six catalysts were prepared by the procedure described above: Ag and Au monometallics, and four Ag-Au bimetallics, with theoretical Au/(Au + Ag) atomic ratios of 0.5, 0.8, 0.9, and 0.95, respectively. For all of them, the total metal loading was always close to 2%wt. The catalysts prepared were named: Au and Ag the monometallic samples, and AgAu(X) the bimetallic ones, where X is the Au/(Ag + Au) theoretical atomic ratio.

2.2. Physicochemical characterization

The actual amount of Ag and Au in the calcined samples were determined by inductively coupled plasma (ICP), using a Perkin Elmer OPTIMA 2100 equipment. The specific BET surface area (S_{BET}), BET pore volume (Vp) and medium pore diameter (dp) of the samples were determined by double isotherm method, using N_2 physisorption, at 77 K, in a Micromeritics ASAP 2020 sorptometer.

X-ray photoemission spectroscopy (XPS) analyses were performed in a SPECS multi-technique apparatus, equipped with a dual Mg/Al X-Ray source and a PHOIBOS 150 hemispherical analyzer, operated in fixed transmission mode (FAT). The XPS spectrums were obtained with the Mg anode operated at 200 W (monochromatic Kα1 radiation 1253.7 eV) and a fixed analyzer pass energy of 30 eV. The solid calcined samples were pretreated in-situ under vacuum at 120 °C for 10 min for degassing. The chamber pressure during the analysis was 2.10^{-8} mbar. The spectral data obtained were processed using Casa-XPS software, and energy corrections were made using C1s (284.5 eV) as reference.

For electron microscopy observations, a sample of calcined precursor powder was dispersed in milli-Q water by 5 min sonication in an ultrasonic bath. A drop of this suspension was applied to a copper grid (holey-200 mesh) coated with carbon film, and was allowed to dry in air. Aberration corrected scanning transmission electron microscopy (Cs-corrected STEM) images were acquired using a high angle annular dark field detector (HAADF) in a FEI XFEG TITAN electron microscope. The Super-Twin® objective lens operated at 300 kV allowed a point-to-point resolution of 0.240 nm A HAADF detector enabled the acquisition of STEM images with atomic number contrast (Z-contrast). Elemental analysis of the samples was carried out with an Energy Dispersive X-ray Spectroscopy detector (EDAX) in the scanning mode.

2.3. Catalytic activity tests

A thermostatized double-walled glass reactor was employed to perform the aqueous-phase oxidation of LA (Aldrich, 99%) at atmospheric pressure. The reactor was loaded with 300 mL of distilled water and appropriate amounts of LA and catalyst to achieve a w/n° ratio of 30 or 15 $g{\cdot}mol^{-1}$. The resulting initial LA concentration (C°_{LA}) was 0.111 $mol{\cdot}L^{-1}$. Then, air was bubbled through the reaction mixture at a constant flow rate of 500 $ml{\cdot}min^{-1}$. The pH of the solution was adjusted and maintained constant at 9 ± 0.1 by an automated system that continuously added a 1.0 N NaOH aqueous solution. Catalytic tests were performed at different temperatures (from 25 °C to 65 °C). Catalysts particle sizes were sieved between 10 and 50 μm before loading to the reaction media, and the obtained slurry was constantly stirred at 900 rpm to avoid transfer limitations by external and internal mass diffusion during LA oxidation. Samples of reaction mixture were collected periodically and analyzed using a Shimadzu HPLC equipped with a refraction index detector. Separation of LA and LB was performed with a Phenomenex™ column (Phenosphere 5 μm, NH2, 80 Å, 250 mm x 4.60 mm) and a 60/40 acetonitrile-sodium phosphate buffer (50 $mmol{\cdot}L^{-1}$, pH = 5.0) as a mobile phase. All solvents were HPLC grade and the mobile phases were filtrated through a 0.22 μm nylon filter. In all cases, only LA and LB were detected and quantified: the mass balance always closed around 98% or higher. After each activity test, a portion of the slurry was recovered from the reaction medium, the catalyst powder was separated by filtration, and the aqueous phase filtrated was analyzed by ICP, in order to determine whether there is Au and/or Ag leaching or not.

Table 1
Textural properties and chemical composition for the bulk and the surface of $AuAg/Al_2O_3$ calcined samples.

Sample	S_{BET}[a] ($m^2 \cdot g^{-1}$)	Vp[b] ($cm^3 \cdot g^{-1}$)	W_M[c] (%wt)		Au/(Ag + Au) atomic ratios	
			Ag	Au	ICP	XPS
Au	180	0.47	–	2.1	1	1
AgAu(0.95)	193	0.46	0.06	1.92	0.95	≈1
AgAu(0.9)	177	0.45	0.12	1.81	0.89	0.55
AgAu(0.8)	193	0.49	0.28	1.69	0.77	0.38
AgAu(0.5)	201	0.48	0.74	1.2	0.47	0
Ag	193	0.49	1.98	–	0	0

[a] Specific surface area determined by the BET method.
[b] Volume pore determined from the N2 isotherm by BJH method.
[c] Metal content determined by ICP and expressed as percentage of $g_{metal}/g_{catalyst}$.

3. Results and discussion

3.1. Physicochemical characterization

The results from the textural analysis are presented in Table 1. For all samples, the specific surface BET areas (S_{BET}) are between 180 and 200 $m^2 g^{-1}$, analogous to the calcined original Al_2O_3 support (190 $m^2 g^{-1}$). The major deviations from the S_{BET} of Al_2O_3 were as much as -7% for the AgAu(0.9) and +6% for the AgAu(0.5). The pore volume (Vp) of all the samples are also similar to that of the Al_2O_3 support (0.49 $cm^3 g^{-1}$), and the major deviation is as much as 4% for the Au monometallic sample. No differences in pore diameter between the samples and the support were observed (results not presented here). Therefore, the textural properties of the support are not affected by the precipitation-deposition process and the subsequent calcination at 500 °C. Table 1 also shows the actual metallic content (w_M) of Ag and Au for each sample, determined by ICP, and the bulk Au/(Ag + Au) atomic ratios calculated from these experimental values. It was verified that the total metallic content in all the samples was approximately 2% wt, as expected. Therefore, it can be established that the preparation procedure and the individual amounts of Ag and Au added were appropriate to achieve the atomic Ag-Au ratios required for the final catalyst.

The XPS spectra corresponding to the Au-4f binding energy level are presented in Fig. 1(a–c), and the corresponding to the Ag-3d energy level in Fig. 1(d–f). Deconvolution of these XPS spectra were carried out assuming two and four peaks, in order to confirm if metal and oxidized Au and Ag species are simultaneously present on the catalyst surface. It was concluded that, in any case, only signals that can be assigned to metallic species were detected. These results are in very good agreement with those found in previous works [21]. For the Au monometallic and AgAu(0.9) bimetallic samples, a very good fitting was obtained with only the doublet peak characteristic of metallic Au at 82.9 eV for the 4f(7/2) and 86.6 eV for 4f(5/2) [22,23]. In addition, no binding energy displacement or changes in the intensities of the peaks assigned to Au-4f were observed, which suggests that the Au electronic sate and the metallic dispersion are similar in both samples. However, the surface Au/(Au + Ag) ratio calculated was significantly lower than the bulk one (Table 1), which indicates a clear enrichment in Ag over the bimetallic nanoparticles surface. Unexpectedly, for the AgAu(0.5) bimetallic sample, no signal assignable to Au species was observed (Fig. 1c), which would prove that no Au is accessible or exposed at the surface. In the Ag-3d region, only a doublet peak at 368.4 eV and 374.4 eV was observed (Fig. 1(d–f)), characteristic of 3d(5/2) and 3d (3/2) energy levels of metallic Ag, respectively [22]. The relative peak intensities indicate that the Ag surface concentration on AgAu(0.5) sample is higher than that on AgAu(0.9), and even than that on the Ag monometallic sample. This could be due to a higher dispersion of Ag atoms in AgAu(0.5) than in both, the AgAu(0.9) and the monometallic Ag samples. No signal assignable to metallic Ag was detected for AgAu (0.95) (result not shown in this work) probably due to the low content of this element in the sample. Summarizing, the surface Au/(Au + Ag) atomic ratio diminished from 1 to 0 as the bulk Au/(Au + Ag) atomic ratio was decreased from 1 to 0.5 (Table 1). Thus, it can be concluded that there is a superficial enrichment of Ag with respect to the Au, even, no superficial Au was detected in the case of the AgAu(0.5) sample. Therefore, an important amount of Au atoms exposed at the bimetallic surface could be observed only for bulk atomic ratios Au/(Au + Ag) ≥ 0.8.

Fig. 2(a–e) shows STEM-HAADF images of the calcined AgAu(0.5) sample, acquired with different magnifications. At the lowest magnifications (Fig. 2a and b), metallic nanoparticles distributed homogeneously on the surface of the support can be seen. Several images obtained for this sample indicate a narrow particle size distribution for the metallic phase (results not shown here). In a previous work, for an $Au(2\%)/Al_2O_3$ catalyst, it was determined an homogenous narrow distribution of monometallic Au nanoparticle sizes, with an average diameter of 4 ± 1.5 nm [17]. The high-resolution micrographs of the

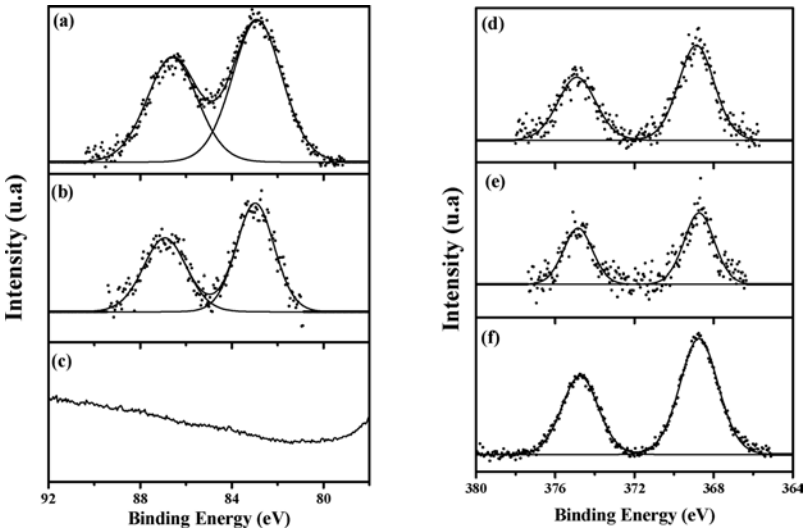

Fig. 1. X-ray photoelectron spectroscopy of calcined samples. Au-4f region: Au (a), AgAu(0.9) (b), AgAu(0.5) (c) and Ag-3d region: Ag (d), AgAu(0.9) (e), AgAu(0.5) (f). Experimental data (points) and XPS-Casa software fittings (lines).

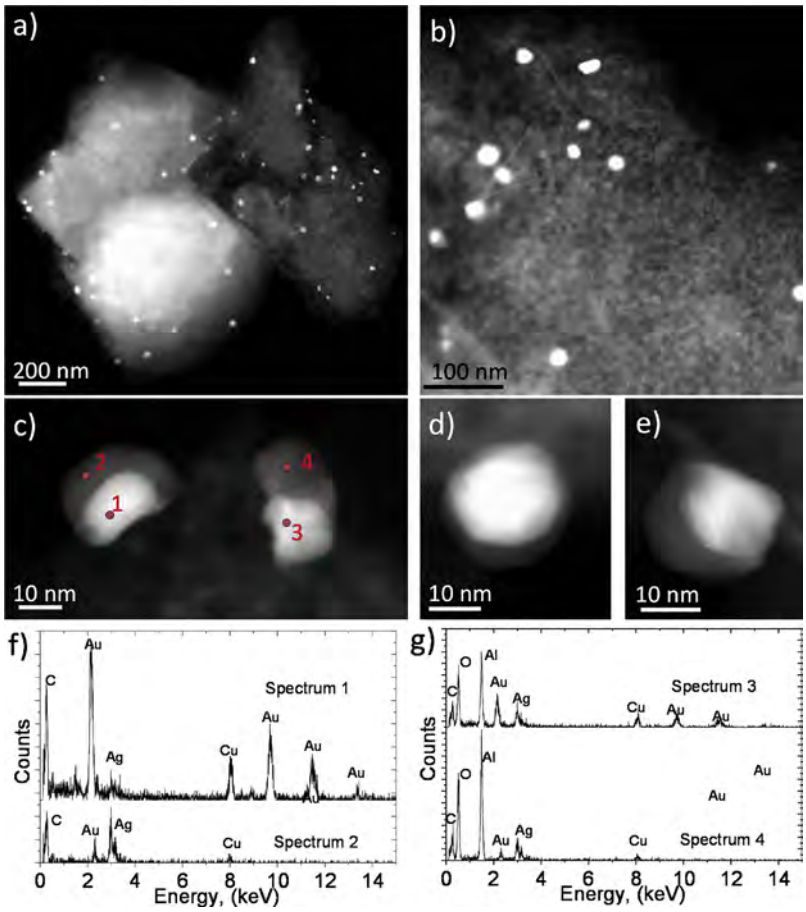

Fig. 2. Micrographs of AgAu(0.5) calcined sample showing bimetallic nanoparticles. (a–b) STEM-HAADF images at different magnifications (AuAg nanoparticles have a bright contrast). (c–e) High resolution STEM-HAADF images showing by Z-contrast a core shell structure (The bright contrast corresponds to Au atoms). (f–g) EDS spectra from locations marked in image (c) confirming a core-shell structure.

AgAu(0.5) sample (Fig. 2c–e), acquired at higher magnifications, show individual nanoparticles with a 10 nm size in order, i.e. somewhat larger than those obtained for monometallic Au catalyst. Besides, the bimetallic Ag-Au nanoparticles have two zones clearly differentiated by their brightness, originated by the high Z-contrast arising from the different atomic number of Ag and Au. These two zones indicate that these nanoparticles have a "core-shell"-type structure. The brightest zone is the nucleus ("core") of the nanoparticles, constituted mainly by the atoms of the highest atomic number, i.e. Au, which was confirmed by EDS analysis (Fig. 2f and g, points 1 and 3). The outer layer ("shell") is mainly formed by Ag, which was confirmed by EDS analysis (Fig. 2f and g, points 2 and 4). These results are in agreement with those obtained by XPS, and verify that Ag is clearly located at the surface of the bimetallic nanoparticles in AgAu(0.5) sample.

STEM-HAADF micrographs corresponding to the calcined AgAu (0.9) sample, obtained with different magnifications, are shown in Fig. 3(a–d). It is observed that metallic nanoparticles are well dispersed on the support surface with a homogenous size distribution ranging from 3 to 8 nm (Fig. 3a and b). EDS analysis revealed only the presence of Au in these nanoparticles (Fig. 3e and f, points 1 to 4) and they do not have a "core-shell" structure. In view of the low Ag content in AgAu (0.9) sample and the results obtained by XPS and EDS analysis, it can be inferred that Ag is almost completely dissolved in the crystalline structure of the Au. Moreover, according to XPS analysis, most of the Ag dissolved in the crystalline network of Au should be mainly at the surface of the metallic nanoparticles. The miscibility of Ag and Au is favored because both metals have similar atomic radius (0.175 nm and 0.179 nm, respectively) and the same crystalline structure (*fcc*), which are necessary condition for the formation of substitutional solid solutions. In addition, metal nanoparticles with a clearly defined arrangement of metallic atoms, ordered in crystallographic planes, could be observed at higher magnifications (Fig. 3c). The high resolution STEM-HAADF images of some individual particles were acquired and one of them is presented in Fig. 4. The interatomic distance obtained, calculated along two of the major directions marked on the nanoparticle, confirmed an interplanar distance of 0.260 nm in both directions (Fig. 4b and c). The interatomic distance for bulk Au {111} family planes is 0.2359 nm. Therefore, the crystalline nano-structures observed in the calcined AgAu(0.9) sample, supported on Al_2O_3, showed a more open structure, and thus, lower density than that of bulk Au. The changes in crystalline structure and density could be associated with the different behaviour of nano-sized structures from that of bulk Au [24]. As a result, Au nano-structures exhibited different physico-chemical properties from those of bulk Au, e.g. chemical activity.

In summary, the metallic supported nanoparticles obtained when the volumetric atomic ratio Au/(Au + Ag) is lower than or equal to 0.5 have a "core-shell" structure, whose core is mainly formed by Au atoms covered by a shell or layer of Ag atoms. On the other hand, the bimetallic samples with Au/(Au + Ag) ratios over 0.5 have a homogeneous distribution of Au-Ag crystalline nanoparticles enriched superficially in Ag. In particular, the AgAu(0.9) sample has a surface Au/Ag ratio close to one, and it is mainly formed by nanoparticles showing an ordered nanostructure (crystal-like) with higher interplanar distances, i.e. showing a lattice expansion, than those of Au bulk.

The results obtained from the characterization of mono and bimetallic Au-Ag samples, prepared by precipitation-deposition method at controlled pH, can be explained by the Ag migration over the support surface and its subsequent diffusion onto the structure of the Au nanocrystallites in the calcination step. It seems that during the two precipitation steps, the corresponding Ag and Au precursors are separately deposited as nanoparticles on the support (Al_2O_3). During the calcination, these precursors are decomposed and, then, Ag atoms

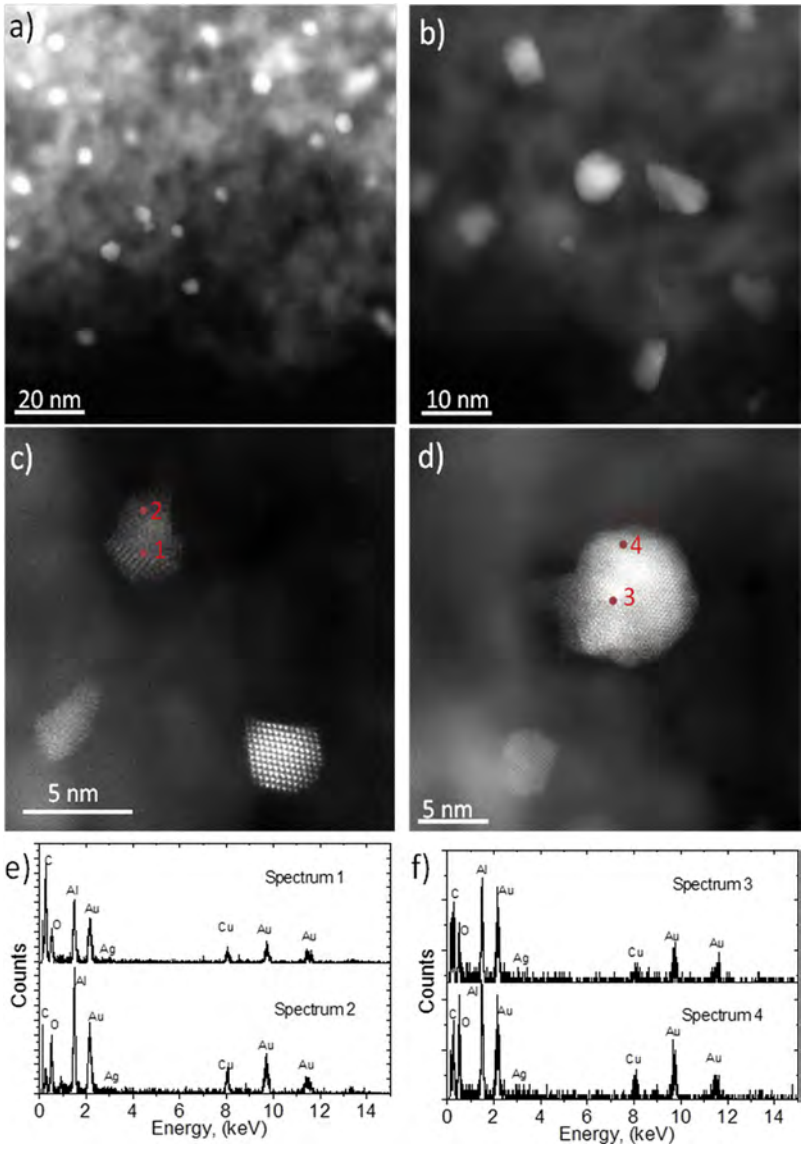

Fig. 3. Micrographs of AgAu(0.9) calcined sample showing bimetallic nanoparticles. (a–b) STEM-HAADF images at different magnifications (AuAg nanoparticles have a bright contrast). (c–d) High resolution STEM-HAADF images showing by Z-contrast a crystalline and alloyed structure is obtained. (e–f) EDS spectra from locations marked in images (c–d) confirming an alloyed structure.

migrate over the support surface, reaching the Au nanoparticles and diffusing very slowly in its crystalline structure. If the Ag content in the sample is low, the Ag atoms can be easily diluted in the network of the Au crystalline nanoparticles. As a result, a bimetallic surface rich in Ag atoms, dispersed in the crystalline structure of Au nanoparticles can be obtained. If the Ag content in the sample is high, and assuming that Ag diffusion in Au network is slower than its migration over the support, it is likely that an important amount of Ag remains covering the Au nanoparticle surface, which is in agreement with XPS results for the sample with Au/(Au + Ag) = 0.5, and confirmed by STEM-HAADF.

3.2. Catalytic tests

3.2.1. Activity of mono and bimetallic Au-Ag samples

All the calcined samples prepared for this work have been tested in the aqueous oxidation of LA to lactobionic acid (LB). The LA conversion after 20 min and 50 min reaction at 65 °C, which correspond to w·t/n° equal to 600 and 1500 g·min·mol^{-1}, respectively, is shown in Fig. 5a. It was observed that Ag and AgAu(0.5) catalysts were practically not active in LA oxidation, since LA conversion was always below 5%, and no LB was observed as a reaction product. The color of these two samples changed from ivory-white or lilac, respectively, to dark brown during LA oxidation, which indicates some kind of surface modification. The very low LA conversion observed for the samples whose metallic surface is mainly composed of Ag atoms (bulk ratio Au/(Au + Ag) ≤ 0.5) could be attributed to the following facts : 1) rich-Ag metal surfaces have low activity for LA oxidation; 2) Ag-based catalysts are deactivated very quickly under the reaction conditions used in this work. Some of the causes of this deactivation could be: 1) strong adsorption of LA and/or LB on the Ag metallic surface sites; 2) superficial oxidation of Ag by the O_2 dissolved in the aqueous solution, which would be in agreement with the color change observed in the catalysts during the reaction.

On the other hand, the Au monometallic and the bimetallic catalysts AgAu(0.95), AgAu(0.9), and AgAu(0.8) showed high activity in LA oxidation, reaching a total LA conversion after 60–120 min. For instance, at 50 min (w·t/n° = 1500 g·min·mol^{-1}) the LA conversion over AgAu(0.9) catalyst was higher than 90%, while it reached 60–70% with Au, AgAu(0.95) and AgAu(0.8) (Fig. 5a). At 20 min (w·t/n° = 600 g·min·mol^{-1}) the activity pattern for Au monometallic and Au-Ag

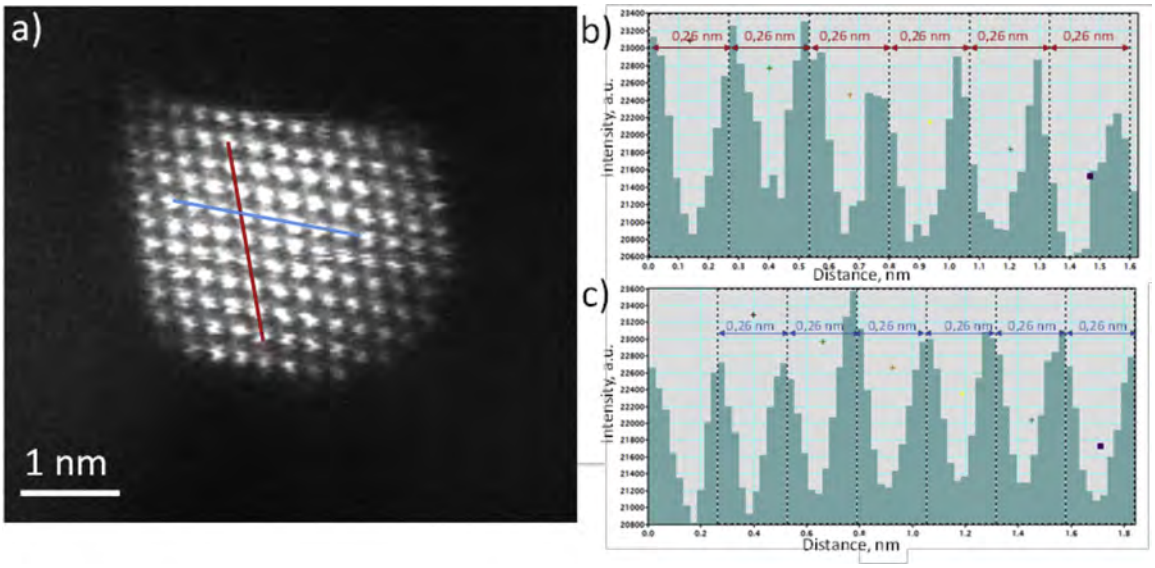

Fig. 4. Micrograph of AgAu(0.9) calcined sample and interatomic distance between two major crystallographic family planes. (a) High resolution STEM-HAADF images of a AuAg bimetallic nanoparticles showing crystallographic planes. (b–c) Interatomic distances calculated along the directions marked on (a).

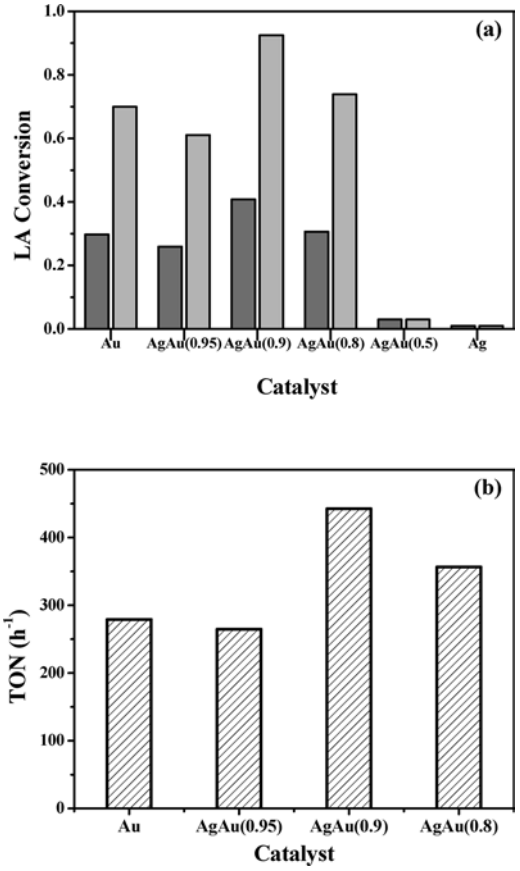

Fig. 5. Catalytic activity of the calcined catalysts prepared. (a) Lactose conversions after 20 min (600 g·min·mol^{-1}) (■), after 50 min (1500 g·min·mol^{-1}) (■). (b) Initial Turn Over Number (TON) for the active catalysts. Reaction conditions: 65 °C, 1 atm (0.21 atm O_2), w/n° = 30 g·mol^{-1}, $C°_{LA}$ = 0.111 mol·L^{-1}, 900 rpm.

bimetallic catalysts is the same as that observed at 1500 g·min·mol^{-1}. Therefore, at 65 °C, the maximum activity was obtained with AgAu(0.9) catalyst, with a bulk atomic ratio Au/(Au + Ag) = 0.9, and a surface ratio of 0.55 as established by XPS (Table 1). After the activity tests, the reaction medium was separated from the solid catalysts and analyzed by ICP (results not shown in this work), verifying that Au and/or Ag leaching was not taking place. In addition, the color of these catalysts did not change during the LA oxidation to LB.

To study LA oxidation with AgAu bimetallic catalysts, the initial LA oxidation rates (r°, mmol·g^{-1} h^{-1}) were estimated by performing the numerical derivative from the curves of LA conversion (X_{LA}) as a function of (w·t/n°). From these initial reaction rates (i.e., at zero min), the initial turnover numbers (TON in h^{-1}) were estimated (Fig. 5b). The TON pattern obtained is similar to the one obtained for LA conversion (Fig. 5a): AgAu(0.9) > AgAu(0.8) > Au ≈ AgAu(0.95). These results show that Au and AgAu(0.95) catalysts have similar catalytic activity and prove that the addition of very small Ag amounts to the monometallic Au catalyst was not enough to modify significantly the catalytic performance of the Au surface. However, an important increase in activity was observed for the AgAu(0.9) catalyst (Fig. 5b). In this case, the Ag content was enough to have a significant influence on the activity of the bimetallic Ag-Au catalyst. However, when the Ag content in the bimetallic catalyst increased from 0.1% in AgAu(0.9) to 0.28 wt% in AgAu(0.8), the initial catalytic activity decreased by almost 20%. For higher Ag contents, very low activity in aqueous-phase LA oxidation was observed. This trend agrees with the important surface enrichment on Ag atoms for these bimetallic catalyst determined by XPS. It was found that the surface atomic ratio Au/(Ag + Au) varies from 0.55 in AgAu(0.9) to practically zero in AgAu(0.5). This implies that a similar Au and Ag atomic surface concentration is necessary to obtain a catalyst more active in LA oxidation. For the AgAu(0.8) sample, the Au/(Ag + Au) surface ratio established from XPS analysis was 0.38, i.e., Ag surface concentration is higher than Au surface concentration, which results in a surface less active for LA oxidation. Finally, AgAu(0.5) and Ag monometallic samples, in which only Ag is exposed on the surface, showed no activity in the LA oxidation. These results indicate that there is an important synergistic effect between Au and Ag in the bimetallic AgAu(0.9) sample whose surface ratio is Au/(Au + Ag)≅0.5.

In some studies on CO oxidation with Ag-Au catalysts, it was proposed that the Au surface sites activate the CO molecules while Ag surface sites activate the O_2 molecules [25–27]. On the other hand, it was shown that the adsorption of O_2 on the surface of Au is very weak and is the limiting stage in the oxidation of LA to LB on monometallic Au catalyst [17]. Thus, it can be inferred that the presence of Ag favors the adsorption of O_2 on the surface of bimetallic AgAu particles. In our

case, it is likely that LA molecules get activated through interaction between metallic Au sites and the carbonyl group, while Ag chemisorbs and activates O_2 molecules [28]. The proximity of metallic Ag and Au sites would favor the interaction between the molecules of LA and O_2 chemisorbed in neighbor sites and, thus, the oxidation of LA to LB. Therefore, it is expected that interaction between LA and O_2 would be maximum for an atomic surface ratio Ag/Au close to 1, which is the case of AgAu(0.9) catalyst. The surface atomic ratio Ag/Au becomes different to 1 as the bimetallic nanoparticles are either more diluted or richer in Ag, thus the probability of having LA and O_2 molecules adsorbed in neighbor metal sites, over the bimetallic Ag-Au surface, diminishes. This synergistic effect between Au and Ag would be lower in AgAu(0.95) and AgAu(0.8) than in AgAu(0.9), and null in the case of AgAu(0.5), in which surface Au/(Ag + Au) = 0.

To summarize, the most active catalyst of this series was AgAu(0.9). This behavior could be explained by the fact that the surfaces of bimetallic nanoparticles are formed by Ag and Au atoms in equal concentration. An atomic Au/Ag ratio of one seems to be the optimum to obtain the highest yield and selectivity to LB in aqueous-phase LA oxidation. As the Ag content was increased, Au particles were completely covered by Ag on the surface. These Ag-Au nanoparticles have a core-shell structure, in which the nucleus is predominantly formed by Au atoms covered by a shell of Ag. These types of particles are not active for LA oxidation.

3.2.2. Influence of reaction temperature

The influence of the reaction temperature on the activity was studied with the Au based and the three bimetallic catalysts which are active in the aqueous-phase LA oxidation, i.e.: Au, AgAu(0.95), AgAu (0.9) and AgAu(0.8). Additional experiments were carried out at 25–65 °C with a w/n° ratio of 15 g·mol^{-1}, under the conditions previously described. Fig. 6 shows the evolutions of LA conversion as a function of w·t/n° and the time at 25 °C (a), 45 °C (b), and 65 °C (c). At 65 °C, except for AgAu(0.95), LA conversion reached 100% after about two hours of reaction or less. On the other hand, at 45 °C, only the Au and AgAu(0.9) catalysts reached 100% conversion after a similar reaction time, while the others reached 50% conversion as maximum. Finally, at 25 °C, none of the catalysts reached 100% LA conversion over the reaction time analyzed. Considering LA conversion at 100 min (w·t/n° = 1500 g·min·mol^{-1}), the pattern obtained at 65 °C (Fig. 6c) was: AgAu(0.9) > Au ≈ AgAu(0.8) > AgAu(0.95), which is in agreement with the maximum activity previously determined (Fig. 5). When the reaction temperature was 45 °C (Fig. 6b), this pattern was modified as follows: AgAu(0.9) ≈ Au > AgAu(0.8) ≈ AgAu(0.95). Finally, at 25 °C (Fig. 6a) the LA conversion pattern was: Au > AgAu(0.9) ≈ AgAu(0.95) > AgAu(0.8). This change on the activity patterns shows the influence of temperature on the rate of LA oxidation, which is different for each bimetallic catalyst.

In order to obtain evidence about the reaction temperature effect on the activity of each catalyst, the LA oxidation rates (r, mol·g^{-1} min^{-1}) were estimated for each run between 0 and 40 min. The reaction rate estimates obtained were plotted as a function of the reaction time (Fig. 7). It was determined that r is almost constant at each temperature and with the four catalysts. This apparent zero order on LA concentration was already observed and explained for Au monometallic catalyst in a previous work [17]. For each temperature and catalyst, the LA oxidation rates estimated at time zero ($r°$) were used to perform a study on temperature dependence of the kinetic rate constant (k). For this purpose, we considered a kinetic expression for r corresponding to a pseudo-homogeneous model (Eq. (1))

$$r = k_{(T)} \times (C_{O2(dis)}) \times (C_{LA(dis)})^m \quad (1)$$

Where $C_{LA(dis)}$ is the LA concentration measured by HPLC, m is the reaction order respect to LA, and $C_{O2(dis)}$ is the oxygen (O_2) concentration in the aqueous phase assuming order 1 respect to O_2. It was assumed that the solubility of O_2 was only a function of temperature and, therefore, its concentration in aqueous phase was calculated by applying Henry's law, given by Eq. (2).

$$C_{O2(dis)} = \bar{p}_{O2} \Big/ \hat{H}^{O2}_{(T)} \quad (2)$$

Where $\bar{p}_{O2}$ is the O_2 partial pressure in the gas phase, considered constant and equal to 0.21 atm, and $\hat{H}^{O2}_{(T)}$ the Henry constant for O_2 dissolved in water, which is a function of temperature, according to Eq. (3).

$$\hat{H}^{O2}_{(T)} = 1000 \bullet MW_{O2} \bullet (a + b \bullet T) \quad (3)$$

Where MW_{O2} is the molar weight of O_2, a and b are the Henry constant for O_2 in water, (a = 0.0126 atm·l·mg^{-1} and b = 5.56·10^{-4} atm·l·mg^{-1} °C^{-1}), and T is the reaction temperature in °C [29,30].

Using the relationship given in Eq. (2), and considering the initial reaction conditions, i.e., zero time; Eq. (1) can now be expressed as Eq. (4):

$$r^0 = k_{(T)} \times \left(\bar{p}_{O2} \Big/ \hat{H}^{O2}_{(T)} \right) \times (C^0_{LA(dis)})^m \quad (4)$$

Where $\bar{p}_{O2}$ and $[C°_{LA(dis)}]^m$ are constant for all the experimental conditions analyzed. In this way, it is possible to estimate the kinetic constant $k_{(T)}$ from the $r°$ for each temperature and catalyst by linear regression.

The apparent activation energies (Ea) and frequency factors (A) for each catalyst were estimated via an Arrhenius function by plotting ln [$k_{(T)}$] as a function of 1/T (Table 2). The Au monometallic sample showed the smallest Ea of the catalyst series (29.5 KJ·mol^{-1}), which was practically half of the highest one for the AgAu(0.8) (54.1

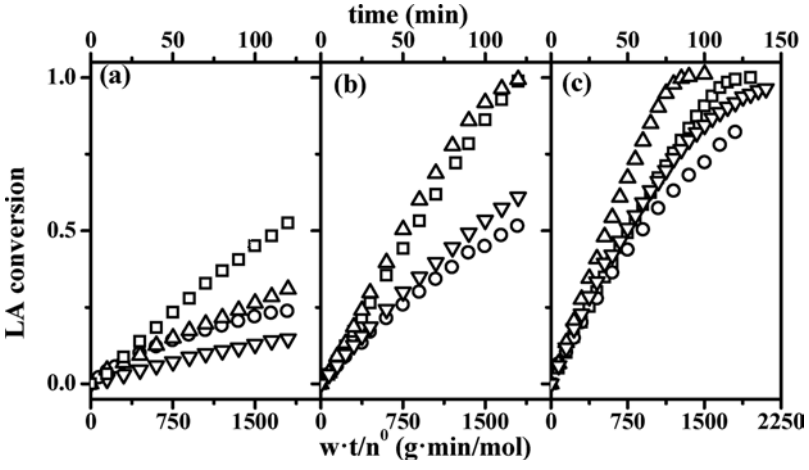

Fig. 6. Lactose conversion as function of (w·t/n°) parameter and temperature: 25 °C (a), 45 °C (b), 65 °C (c), □ Au, ○ AgAu(0.95), △ AgAu(0.9), ▽AgAu(0.8). Reaction conditions: 1 atm (0.21 atm O_2), w/n° = 15 g·mol^{-1}, C°$_{LA}$ = 0.111 mol·L^{-1}, 900 rpm.

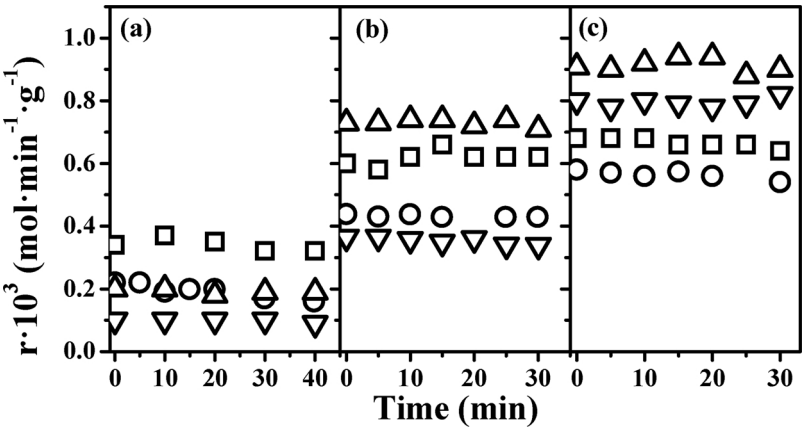

Fig. 7. Lactose oxidation rate (r) for the active catalysts as function of reaction time and temperature: 25 °C (a), 45 °C (b), 65 °C (c), □ Au, ○ AgAu(0.95), △ AgAu(0.9), ▽ AgAu(0.8). Reaction conditions: 1 atm (0.21 atm O_2), w/n° = 15 g·mol^{-1}, $C°_{LA}$ = 0.111 mol·L^{-1}, 900 rpm.

Table 2
Estimates for frequency factors and apparent activation energies for the active catalysts in lactose (LA) oxidation.

Catalyst	A[a] (L·g^{-1}·h^{-1})	Ea[b] (KJ·mol^{-1})
Au	$1.14 \cdot 10^{7}$	29.5
AgAu(0.95)	$4.71 \cdot 10^{7}$	33.8
AgAu(0.9)	$2.92 \cdot 10^{9}$	44.1
AgAu(0.8)	$8.06 \cdot 10^{10}$	54.1

[a] Frequency factor from Arrhenius law.
[b] Apparent energy activation from Arrhenius law.

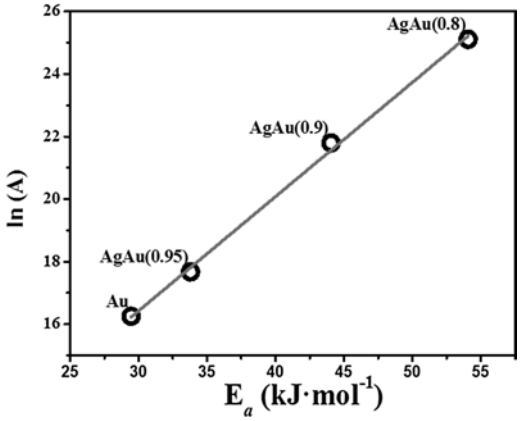

Fig. 8. Compensation effect between the Arrhenius frequency factor (A) and the apparent activation energy (Ea). Reaction conditions: 1 atm (0.21 atm O_2), w/n° = 15 g·mol^{-1}, $C°_{LA}$ = 0.111 mol·L^{-1}, 900 rpm.

KJ·mol^{-1}). Similarly, A increased four orders by increasing the Ag content of the catalyst from the monometallic to the AgAu(0.8). Hence, both Ea and A estimates increased with the Ag content of the bimetallic catalyst. The linear correlation obtained for the [ln (A)] as a function of Ea (Fig. 8), for the four catalysts active in the aqueous-phase LA oxidation, confirms this trend. It can be observed that there is a compensating effect between Ea and A, on the rate kinetic constant, which was already mentioned for other oxidation reactions [31]. In this way, a particular Au/(Au + Ag) ratio can be considered to have the appropriate combination of Ea and A, which resulted in the most active catalyst. This explains why the catalyst AgAu(0.9) was the most active of this series, since the Ea was 1.5 times higher than the one estimated for the monometallic Au catalyst, but the frequency factor A is two orders higher. It can be argued that the surface enrichment of Ag observed in this catalyst increased the activation energy (Ea) necessary for the reaction to occur. But, in turn, it notably improved the effectiveness or frequency of the molecular shocks between the reactant molecules and the surface active sites on the catalyst, to convert them in the product molecules. This important rise of the A factor is in agreement with the former proposal. Au chemisorbs LA molecules and Ag activates O_2 molecules, favoring the interaction and subsequent reaction between the adsorbed species in neighbor metal sites. As the Ag surface concentration augments, the probability of interaction between activated LA and O_2 molecules also increases, and so does the A frequency factor. In this way, it is possible to compensate the negative effect of the activation energy on the LA oxidation, until an optimum in Au/Ag ratio can be reached.

4. Conclusions

Bimetallic AgAu/Al_2O_3 catalysts with different Au/(Au + Ag) atomic ratios were prepared and tested in an aqueous-phase lactose oxidation. The nanostructure and activity of the bimetallic Au-Ag-based catalysts strongly depends on the Au/(Au + Ag) ratio. For an atomic Au/(Au + Ag) ratio of 0.5 or lower, bimetallic nanoparticles with core-shell structure were obtained, in which the Ag is located preferentially in the periphery of the particles, completely covering the Au located in the core of them. This type of particles, as well as the monometallic catalyst of Ag, are very little active in the lactose oxidation. For Au/(Au + Ag) ratios higher than 0.5, bimetallic nanoparticles with surface enrichment in Ag were obtained; for these, the Au is accessible to the reactant molecules. These particles are more active in the selective lactose oxidation to lactobionic acid than Au monometallic, being the catalyst, AgAu(0.9)/Al_2O_3 with an Au/(Au + Ag) = 0.9, the most active of the series. This catalyst has a surface Au/(Au + Ag) ratio close to 0.5, and it is formed by nanoparticles showing an ordered nanostructure (crystal-like) with higher interplanar distances than those of Au bulk. From the kinetic study, it was determined that there is a compensating effect between the activation energy and the frequency factor that explains why AgAu(0.9)/Al_2O_3 catalyst is the most active of the series.

Acknowledgments

The authors thank the National University of the Litoral, CONICET and ANPCyT for the financial support. They are also grateful to ANPCyT for the purchase of the multi-technical analysis instrument (SPECS PME8-2003) and to LMA-INA-UNIZAR for the analysis by transmission electron microscopy. They also thank M. Herman for her help with English revision of the manuscript.

References

[1] A. Corma, S. Iborra, A. Velty, Chemical routes for the transformation of biomass into chemicals, Chem. Rev. 107 (2007) 2411–2502.

[2] P. Gallezot, Catalytic routes from renewable to fine chemical, Catal. Today 121 (2007) 76–91.
[3] P. Imhof, J.C. van der Waal (Eds.), Catalytic Process Development for Renewable Materials, Wiley-Vch, 2013.
[4] P.N. Amaniampong, X. Jia, B. Wang, S.H. Mushrif, A. Borgna, Y. Yang, Catalytic oxidation of cellobiose over TiO_2 supported gold-based bimetallic nanoparticles, Catal. Sci. Technol. 5 (2015) 2393–2405.
[5] A. Abbadi, K.F. Gotlieb, J.B.M. Meiberg, H. van Bekkum, Selective chemo-catalytic oxidation of lactose and/of lactobionic acid towards 1-carboxylactulose (2-keto-lactobionic acid), Appl. Catal. A Gen. 156 (1997) 105–115.
[6] M. Besson, F. Lahmer, P. Gallezot, P. Fuertes, G. Flèche, Catalytic oxidation of glucose on bismuth-promoted palladium catalysts, J. Catal. 152 (1995) 116–121.
[7] J. Zelin, C.I. Meyer, S.A. Regenhardt, V. Sebastian, T.F. Garetto, A.J. Marchi, Selective liquid-phase hydrogenation over copper-supported metallic nanoparticles, Chem. Eng. J. 319 (2017) 48–56.
[8] J. Kuusisto, A. Tokarev, E.V. Murzina, M.U. Roslound, J.P. Mikkola, D.Y. Murzin, T. Salmi, From renewable raw materials to high value-added fine chemicals-catalytic hydrogenation and oxidation of d-lactose, Catal. Today 121 (2007) 92–99.
[9] L.F. Gutiérrez, S. Hamoudi, K. Belkacemi, Lactobionic acid: a high value-added lactose derivative for food and pharmaceutical applications, Int. Dairy J. 26 (2012) 103–111.
[10] M. Comotti, C. Della Pina, E. Falletta, M. Rossi, Aerobic oxidation of glucose with gold catalyst: hydrogen peroxide as intermediate reagent, Adv. Synth. Catal. 348 (2006) 313–316.
[11] P. Budtz, J. Vindelev, P. Ashie, M. Nordkvist, Enzymatic process for obtained increased yield of lactobionic acid, Canadian Patent WO(2005)104859 A3.
[12] A.V. Tokarev, E.V. Murzina, J.P. Mikkola, J. Kuusisto, M.L. Kustov, D.Y. Murzin, Application of in situ catalyst potential measurements for estimation of reaction performance: lactose oxidation over Au and Pd catalysts, Chem. Eng. J. 134 (2007) 153–161.
[13] E.V. Murzina, A.V. Tokarev, K. Kordas, H. Karhu, J.P. Mikkola, D.Y. Murzin, D-Lactose oxidation over gold catalysts, Catal. Today 131 (2008) 385–392.
[14] K. Belkacemi, S. Hamoudi, Chemocatalytic oxidation of lactose to lactobionic acid over Pd-Bi/SBA-15: reaction kinetics and modelling, Ind. Eng. Chem. Res. 49 (2010) 6878–6889.
[15] L.F. Gutierrez, S. Hamoudi, K. Belkacemi, Selective production of lactobionic acid by aerobic oxidation of lactose over gold crystallites supported on mesoporous silica, Appl. Catal. A Gen. 402 (2011) 94–103.
[16] N. Meyer, M. Devillers, S. Hermans, Boron nitride supported Pd catalysts for the hydrogenation of lactose, Catal. Today 241 (2015) 200–207.
[17] C.I. Meyer, S.A. Regenhardt, J. Zelin, V. Sebastian, A.J. Marchi, A kinetic modeling of the liquid-phase oxidation of lactose over Pt- and Au-supported catalysts, Top. Catal. 59 (2016) 168–177.
[18] T. Benkó, A. Beck, K. Frey, D.F. Srankó, O. Geszti, G. Sáfrán, B. Maróti, Z. Schay, Bimetallic Ag-Au/SiO_2 catalysts: formation, structure and synergistic activity in glucose oxidation, Appl. Catal. A Gen. 479 (2014) 103–111.
[19] H. Zhang, N. Toshima, K. Takasaki, M. Okumura, Preparation of Agcore/Aushell bimetallic nanoparticles from physical mixtures of Au clusters and Ag ions under dark conditions and their catalytic activity for aerobic glucose oxidation, J. Alloys. Compd. 586 (2014) 462–468.
[20] M.A. Centeno, K. Hadjiivanov, Tz. Venkov, Hr. Klimev, J.A. Odriozola, Comparative study of Au/Al_2O_3 and Au/CeO_2-Al_2O_3 catalysts, J. Mol. Catal. A Chem. 252 (2006) 142–149.
[21] M. Zacharska, A.L. Chuvilin, V.V. Kriventsov, S. Beloshapkin, M. Estrada, A. Simakovf, D.A. Bulushev, Support effect for nanosized Au catalysts in hydrogen production from formic acid decomposition, Catal. Sci. Technol. 6 (2016) 6853–6860.
[22] National Institute of Standards and Technology, X-ray Photoelectron Spectroscopy Database (Accessed 05 February 2018), https://srdata.nist.gov/xps/Default.aspx.
[23] M.P. Casaletto, A. Longo, A. Martorana, A. Prestianni, A.M. Venezia, XPS study of supported gold catalysts: the role of Au^0 an Au^+ species as active sites, Surf. Interface Anal. 38 (2006) 215–218.
[24] Z. Kolská, J. Říha, V. Hnatowicz, V. Svorcik, Lattice parameter and expected density of Au nano-structures sputtered on glass, Mat. Lett. 64 (2010) 1160–1162.
[25] A. Wang, Y.-P. Hsieh, Y.-F. Chen, C.-Y. Mou, Au-Ag alloy nanoparticle as catalyst for CO oxidation: effect of Si/Al ratio of mesoporous support, J. Catal. 237 (2006) 197–206.
[26] Y. Iizuka, T. Miyamae, T. Miura, M. Okumura, M. Daté, M. Haruta, A kinetic study on the low temperature oxidation of CO over Ag-contaminated Au fine powder, J. Catal. 262 (2009) 280–286.
[27] A. Sandoval, A. Aguilar, C. Louis, A. Traverse, R. Zanella, Bimetallic Au-Ag/TiO_2 catalyst prepared by deposition-precipitation: high activity and stability in CO oxidation, J. Catal. 281 (2011) 40–49.
[28] H. Nakatsuji, Z.-M. Hu, H. Nakai, K. Ikeda, Activation of O_2 on Cu, Ag and Au surfaces for the epoxidation of ethylene: dipped adcluster model study, Surf. Sci. 387 (1997) 328–341.
[29] D.W. Green, R.H. Perry, Perry´s Chemical Engineering Handbook, 8th ed., “Mc. Graw-Hill” Companies Inc., USA, 2008 pp. 2–131.
[30] H.L. Clever, R. Battino, H. Miyamoto, Y. Yampolski, C.L. Young, Oxygen and ozone in water, aqueous solutions, and organic liquids (Supplement to Solubility Data Series Volume 7), J. Phys. Chem. Ref. Data 43 (033102) (2014) 1–209.
[31] T.F. Garetto, E. Rincón, C.R. Apesteguía, Deep oxidation of propane on Pt-supported catalysts: drastic turnover rate enhancement using zeolite supports, Appl. Catal. B: Environ. 48 (2004) 167–174.